



6-2012

Geophysical and Remote Sensing Applications for a Better Understanding of the Structural Controls on Groundwater Flow in the Lucerne Valley, California

Dale R. Dailey
Western Michigan University

Follow this and additional works at: https://scholarworks.wmich.edu/masters_theses



Part of the Geology Commons, Hydrology Commons, and the Remote Sensing Commons

Recommended Citation

Dailey, Dale R., "Geophysical and Remote Sensing Applications for a Better Understanding of the Structural Controls on Groundwater Flow in the Lucerne Valley, California" (2012). *Masters Theses*. 66. https://scholarworks.wmich.edu/masters_theses/66

This Masters Thesis-Open Access is brought to you for free and open access by the Graduate College at ScholarWorks at WMU. It has been accepted for inclusion in Masters Theses by an authorized administrator of ScholarWorks at WMU. For more information, please contact wmu-scholarworks@wmich.edu.



GB
9999
.D355

GEOPHYSICAL AND REMOTE SENSING APPLICATION FOR BETTER
UNDERSTANDING OF THE STRUCTURAL CONTROLS ON
GROUNDWATER FLOW IN THE LUCERNE VALLEY,
CALIFORNIA

by

Dale R. Dailey

A Thesis
Submitted to the
Faculty of The Graduate College
in partial fulfillment of the
requirements for the
Degree of Master of Science
Department of Geosciences
Advisor: Mohammed Sultan, Ph.D.

Western Michigan University
Kalamazoo, Michigan
June 2012

THE GRADUATE COLLEGE
WESTERN MICHIGAN UNIVERSITY
KALAMAZOO, MICHIGAN

Date May 23, 2012

WE HEREBY APPROVE THE THESIS SUBMITTED BY

Dale R. Dailey

ENTITLED Geophysical and Remote Sensing Application for Better Understanding
of the Structural Controls on Groundwater Flow in the Lucerne Valley, California

AS PARTIAL FULFILLMENT OF THE REQUIREMENTS FOR THE

DEGREE OF Master of Science

Geosciences

(Department)



Mohamed Sultan
Thesis Committee Chair

Geology

(Program)



W. Richard Laton
Thesis Committee Member



Bill Sauck
Thesis Committee Member

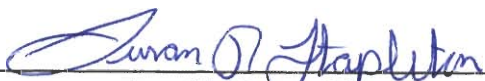


Duane Hampton
Thesis Committee Member



Christopher Schmidt
Thesis Committee Member

APPROVED



Dean of The Graduate College

Date

June 2012

GEOPHYSICAL AND REMOTE SENSING APPLICATION FOR BETTER
UNDERSTANDING OF THE STRUCTURAL CONTROLS ON
GROUNDWATER FLOW IN THE LUCERNE VALLEY,
CALIFORNIA

Dale R. Dailey, M.S.

Western Michigan University, 2012

An integrated study was conducted in the Mojave Basin to investigate the potential role of faults and basement uplifts for groundwater flow in the Mojave Desert. Observations made include: 1) Very Low Frequency (VLF) measurements across mapped (using LIDAR and Geoeye-1 imagery) fault traces showed significant radio field dip angles indicative of presence of shallow sub-vertical, sheet-like conductors; many of the VLF tilt peaks coincided with changes in the magnetic profiles; 2) Vertical Electric Soundings indicate shallow basement west of, and parallel to, the Helendale Fault and deep saturated zones east of the fault/basement outcrop (F/B); and 3) isotopic analyses for groundwater from productive wells, and mountain front and valley springs sampled west of the F/B are less depleted than samples east of the F/B, and show evidence of mixing between aquifers on either side. Findings are consistent with the Helendale Fault channeling groundwater from the San Bernardino Mountains with basement uplifts acting as barriers to lateral groundwater flow.

Copyright by
Dale R. Dailey
2012

ACKNOWLEDGMENTS

I would like to begin by thanking my family and friends that have shown me such tremendous love and support over the past few years as I pursued my Master's Degree. Without their continued dedication and encouragement, I would not be where I am today.

I would also like to thank my advisors: Mohamed Sultan, Bill Sauck, Richard Laton, and Adam Milewski for their help in guiding me through this project and providing their invaluable experience and technical expertise along the way. Christopher Schmidt and Duane Hampton, while not directly involved in the project, were also invaluable sources of help and information, and they also have my gratitude.

Lastly, I would like to thank Mojave Water Agency for the logistical support provided, and Phil Armstrong and the CSUF and WMU Departments of Geology and Geosciences for their help in providing field equipment and technical support. Funding for this project was supplied by Mojave Water Agency and California State University, Fullerton.

Dale R Dailey

TABLE OF CONTENTS

ACKNOWLEDGMENTS	ii
LIST OF TABLES	v
LIST OF FIGURES.....	vi
CHAPTER	
1. INTRODUCTION.....	1
1.1 Project Statement and Location Background	1
1.2 Geologic and Hydrogeologic Setting.....	4
2. METHODOLOGY.....	10
2.1 Methodology Overview.....	10
2.2 Remote Sensing Methods.....	10
2.2.1 Light Detection and Ranging.....	10
2.2.2 GeoEye-1	11
2.2.3 Advanced Spaceborne Thermal Emission and Reflection Radiometer (ASTER).....	12
2.3 Geophysical Methods	12
2.3.1 Very Low Frequency (VLF) Profiles	12
2.3.2 Magnetic Profiles	14
2.3.3 Vertical Electrical Soundings.....	15
2.4 Isotopic Methods	16
2.5 GIS Analyses	17

Table of Contents—continued

CHAPTER	
3. DATA AND DISCUSSIONS	19
3.1 VLF and Magnetic Data	19
3.2 VES Data	27
3.3 Isotope Data	32
4. SUMMARY	39
4.1 Interpretation of Results	39
4.2 Regional Implications	42
REFERENCES	43

LIST OF TABLES

1. List of well and spring samples, including naming schema, specific and general location information, elevation, and isotope data. 35

LIST OF FIGURES

1. Figure 1. Overview of the southern Mojave Desert.....	2
2. Figure 2 (A) Simplified geologic map, (B) Cross Section along line A-A' shown in Fig. 2(A).....	6
3. Figure 3. Location map for our VLF and Magnetic transects, and VES resistivity data	8
4. Figure 4a-c. Selected VLF and Magnetic transects for the northwest portion of the Helendale Fault	21
5. Figure 5d-f. Corresponding VLF and magnetic plots for figure 4a-4c.	22
6. Figure 6a-c. Selected VLF and Magnetic transects for the southeast portion of the Helendale Fault	26
7. Figure 7d-g. Continuation of figure 5, showing corresponding VLF and magnetic plots for figure 5a-5c.	24
8. Figure 8. VES location, apparent resistivity, thickness, and distribution of saturated and unsaturated rock units in areas west and east of the Helendale Fault	29
9. Figure 9. Geoelectric Cross Section along line A-A' in figure 8.....	32
10. Figure 10. Locations of wells and springs sampled for isotopic analysis.....	34
11. Figure 11. Comparison between stable isotope ratios for groundwater samples from wells and springs west, east, and proximal to the Helendale Fault	36

CHAPTER 1

INTRODUCTION

1.1 Project Statement and Location Background

The Mojave Desert occupies areas in southeastern and central California, southern Nevada, southwestern Utah, and northwestern Arizona, in the United States. The southwestern Mojave Desert is characterized by numerous mountain ranges within it including the Tehachapi, the San Gabriel, and San Bernardino that are separated by valleys and inland basins (e.g., Badwater, Owl Canyon, Victor Valley, High Desert, and Rainbow Basin). These mountain ranges and valleys are part of the Basin and Range province, an area witnessing crustal thinning, pull apart basin tectonics (from 17 -22 MA in age though 6-13 MA in age), and lateral displacements across the numerous dextral faults (e.g., Helendale, Lenwood, Lockhart, and Camp Rock) related to the Late Cenozoic tectonics in the area (Dokka, 1990; Dokka, 1983). These dextral fault systems formed secondarily to the San Andreas Fault, due primarily to extension and rotation of the Mojave Fault Block (Dokka, 1990; Dokka, 2001).

The Mojave River Basin, the study area, lies in the extreme southern portion of the Mojave Desert (Fig. 1, Red Watersheds). The basin itself is located in northern San Bernardino County, about 65 km northeast of Los Angeles, California. The basin is the primary water supply for the southern Mojave Desert. Its rapidly growing population (combined population in 1980: 64,685; combined population in

2010: 349,730) has created an ever increasing need for fresh water resources.

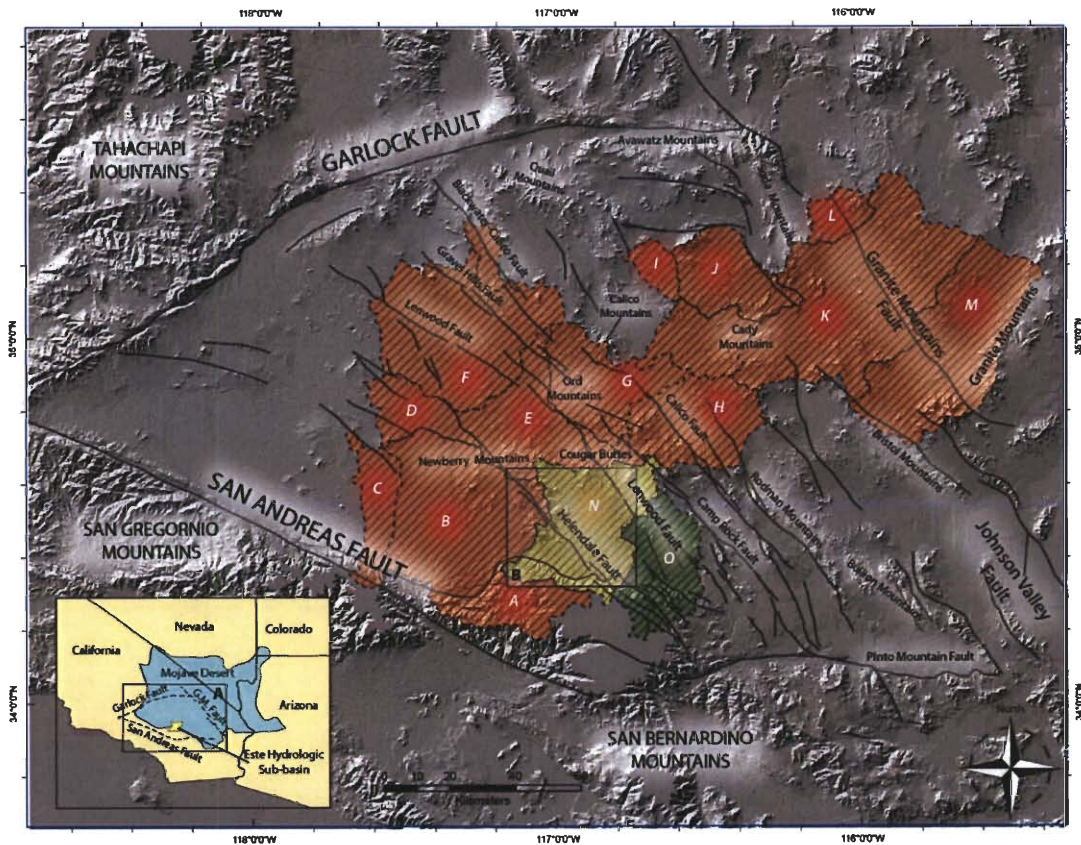


Figure 1. Overview of the southern Mojave Desert. A hill shade has been applied to accentuate topographic features showing the distribution of major: (a) faults (e.g., San Andreas, Garlock), (b) mountain ranges (e.g., Tehachapi, San Gregornio, San Bernardino, and Pinto mountains), (c) subbasins defined by these mountain ranges; labeled “A” through “M”, and (d) aquifers (e.g., Mojave River Regional: red areas; Lucerne Valley: yellow; Johnson Valley: green). Enlargements of the study area covered by Box “B” are shown in Figs 2a, and 3. Inset (lower left corner) shows the areal extent of the Mojave Desert in California, Nevada, Utah, and Arizona and Box “A” outlines the area covered in Fig. 1.

Precipitation in this area averages between 25 and 40 centimeters annually (USGS, 2004; Laton et.al, 2005). Surface water is limited to ephemeral flow during winter and spring storm periods. Runoff and groundwater flow resulting from the

melting of snowpack over the adjacent San Bernardino Mountains constitute the principal source of the groundwater in the southern parts of the Mojave River Basin (Stamos et. al., 2003; Laton et al, 2005; USGS, 2004), whereas the northern and central portions of the basin are largely recharged by groundwater and surface flow from the Cougar Buttes and Granite mountains (Fig. 1), as well as infiltration via the Mojave River floodplain aquifer.

Increasing extraction of groundwater from the Mojave River Basin affected various sections in the basin in varying degrees, The central portions witnessed progressive decline in water levels over the years (20m from 1950-1986), whereas areas proximal to the mountains either did not, or showed significantly less decline (Laton, 2005; Smith and Pimentel, 1998). One popular explanation for the groundwater deficits in the central parts of the basin is that the dextral faults in the area acted as barriers for lateral flow of groundwater from the mountains towards the central parts of the basin (Stamos et al, 2003). A better understanding of how regional and local fault systems interact with the principle aquifers in the Mojave is of key importance in meeting the rising demand for groundwater resources.

In this study, we examine the role of one of the major dextral faults in the area, the Helendale fault and its subsequent splays, as potential barriers to groundwater flow (Stamos et.al, 2003), or as a conduit for groundwater flow (Dailey et. al., 2010; Sultan et. al., 2007). The former widely accepted hypothesis is largely based on the observed water level differences (3-10 m) across each of the Johnson

Valley and Emerson Faults (Lewis, 1972; Trayler and Koczot, 1995; GSI, 2000) and those observed (~40 m) across the Helendale fault in the Central Lucerne Valley area. This explanation is at odds with reported findings elsewhere that suggest that fractured fault planes often act as conduits for groundwater flow (Sultan et. al., 2007; Caine et al., 1996; Gudmundsson, 2001). If such models were applicable to the Helendale, the fault could be channeling groundwater from the San Bernardino Mountains in the south, to the lowlands of the Mojave River Basin in the north, a suggestion that could probably account for an annual groundwater surplus of 300-700 acre feet in the Lucerne Valley Aquifer (Laton et al., 2005) and of 900-1000 acre-feet in the Johnson Valley Aquifer (Kennedy, et al., 2007).

An integrated approach utilizing remote sensing, geophysical, geochemical, and subsurface data was adopted to investigate: (1) the potential role of the Helendale Fault as a barrier for lateral groundwater flow or as a conduit for groundwater flow along its length, and (2) the distribution and nature of barriers for lateral groundwater flow in the study area. The wide distribution of similar structural elements (e.g., strike slip faults) and landforms (mountainous areas and inland basins) in the Mojave Desert makes it likely that our findings could be applicable to many other similar areas in the Mojave Desert.

1.2 Geologic and Hydrogeologic Setting

The Mojave River Basin is characterized by a series of Cenozoic, parallel, northwest trending dextral strike-slip faults which make up the Mojave Desert Fault Block in the eastern California Shear Zone. Their occurrence spans from the San Andreas Fault in the west to the Johnson Valley fault in the east (Fig. 1). The fault system is commonly thought of as a simple shear system with the dextral faults terminating against the cross-cutting Garlock Fault to the north, and the San Bernardino thrust belt in the south (Garfunkel, 1974). This model is contested by more recent research by Dokka, who suggests that the basin is instead a more complex rotational system, with the majority of offset along the faults being attributable to extensional and rotational elements due to movement along the San Andreas Fault (Dokka 1986, 1990). The southern portions of the basin are also characterized by thrust faulting along the San Bernardino mountain belt. The Northeast Mojave Block, located in the northeastern portion of the Mojave Desert, is a separate rotational block of dextral faults, oriented west to east, and trending nearly perpendicular to the majority of other dextral faults in the shear zone (Dokka, 1991).

The southernmost boundary of the Mojave Desert terminates against the San Bernardino Mountain belt. These mountains, along with other smaller mountain belts and outcrops, form the shallow bedrock underlying the Este Hydrologic sub-basin. Bedrock units in the Mojave River Basin consist mainly of Mesozoic granites and gabbros, with sparse dispersions of Tertiary volcanic units in the central and northern portions of the basin. Quaternary alluvial sediments make up the majority of surface

sediments, with additional marine and non-marine sand deposits spread sparsely throughout the basin, generally near the coast or desert playas (Fig. 2a).

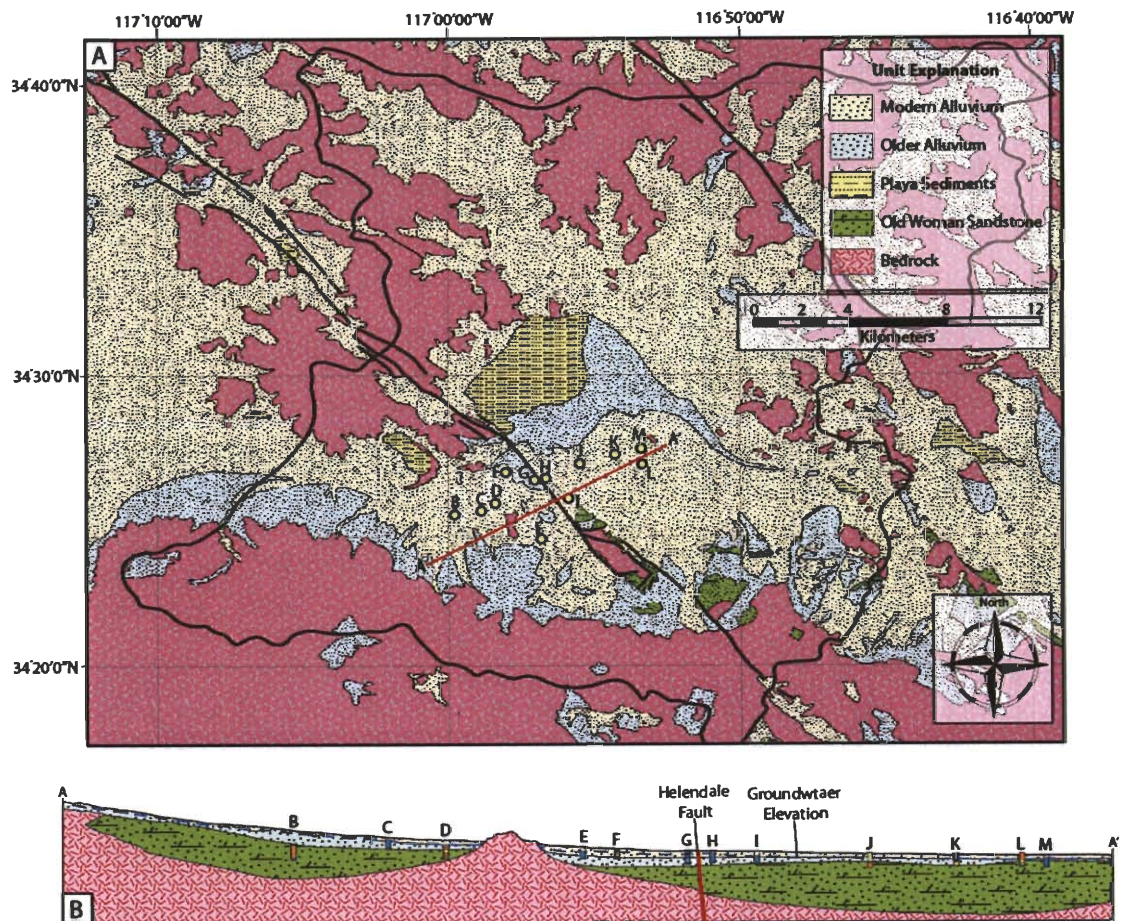


Figure 2.

- (A) Simplified geologic map. This map shows the distribution of the major rock groups, and bedrock ridges (subparallel to Helendale and Lenwood faults) that we infer to extend along their projected length at shallow depths beneath the overlying alluvium.
- (B) A cross section along line A-A' shown in Fig. 2a. Cross section constructed from lithologic and head data extracted from well proximal to the Helendale (yellow circles).

The Lucerne Valley groundwater basin, located in the Este hydrologic sub-basin, is a closed watershed, with no external surface water flowing from the basin (Blazevic and Laton, 2008). The basin contains several shallow bedrock ridges that are proximal and parallel to the dextral fault systems in the valley. The faults originate and/or terminate against the northern and southern mountain ranges. For example, Fig. 1 shows the Helendale Fault originating in the south along the San Bernardino Mountain front, and extending northwest, terminating in the Newberry Mountains. Surficial sediments are derived from the surrounding mountains via weathering and erosion, and carried to the lower portions of the basin via expansive alluvial fan and ephemeral stream systems. The collective alluvial material is comprised of Tertiary sediments and Quaternary stream alluvium, combined with playa, dune, and some landslide deposits (Blazevic and Laton, 2008). The Lucerne valley dry lake represents the topographic low for the sub-basin (86 m amsl) while the mountain peaks to the south represent the topographic high (2513 m amsl).

The Mojave River basin is broken up into a series of smaller sub basins. These subbasins are apparently separated by ridges defined by basement and/or bedrock outcrops and shallow bedrock saddles between the exposed ridges. Examination of Fig. 3 shows that the Lucerne Valley Aquifer in the Este subbasin is separated from the Fifteen Mile Valley Aquifer by a NW-SE trending bedrock ridge. Across some of these ridges and proximal, sub-parallel faults, large differences in water levels were reported. For example, Fig. 2b (located on the previous page)

shows an abrupt drop in water levels in the vicinity of the Helendale Fault. Water levels are not the only features that vary across these topographic ridges and/or faults. Varying groundwater flow directions were reported from aquifers separated by these topographic highs and faults.

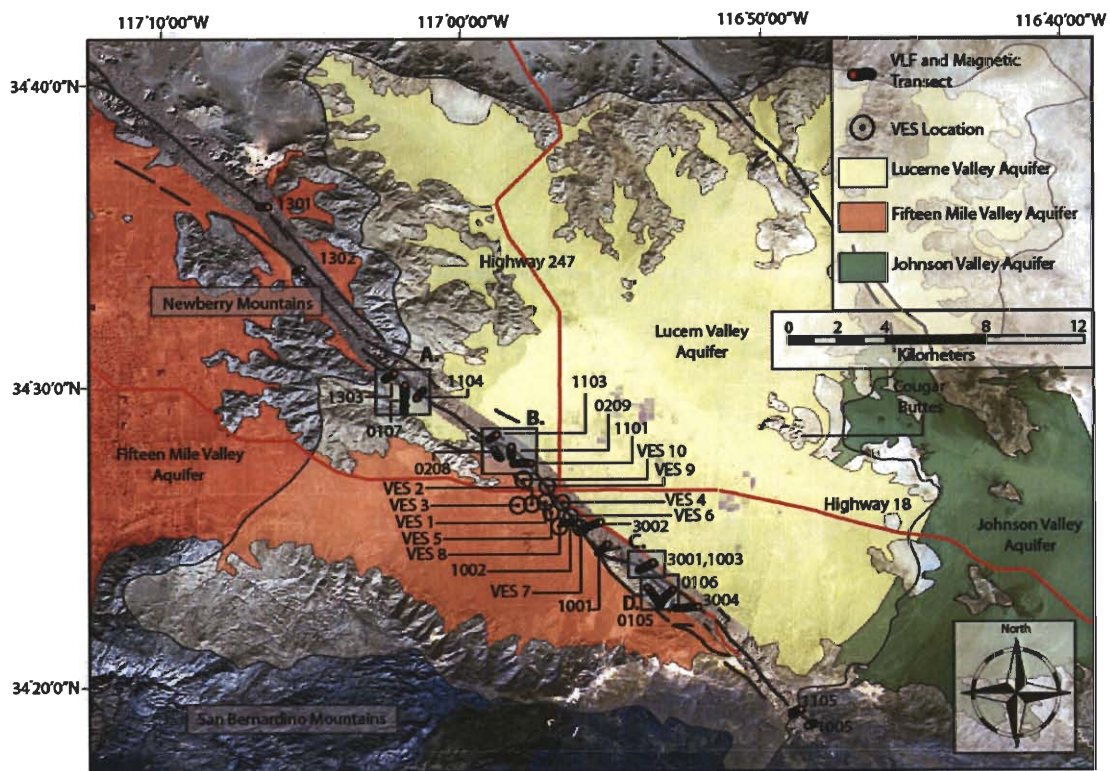


Figure 3. Location map for our VLF and Magnetic transects (thick black lines) and VES resistivity data (open circles). Boxes a, b, c, and d outline locations where findings from VLF data were indicative of presence of conductive subvertical layers.

These shallow aquifers, ranging from 15-90 m in depth (Fig. 2b) in places like Lucerne Valley, are recharged through precipitation and surface runoff during the short rain seasons (Stamos et. al., 2003). Surface runoff consists of both rainfall

runoff following precipitation events, as well as snow melt in the spring from the San Bernardino Mountains. Many of these shallow aquifer systems feed a large central aquifer, known as the Regional Mojave River aquifer. This deeper aquifer is present throughout the Mojave River Basin, underlying several watersheds and subbasins present along the length of the Mojave River (Fig.1). The Regional Aquifer is recharged at the southwest portion of the Este sub-basin west of the Helendale Fault, where it receives incoming surface flow and groundwater carried along the foothills of the San Bernardino Mountains. East and north of the fault, the Este sub-basin is underlain by the Lucerne Valley Aquifer, which is the primary source of groundwater for the residents of Lucerne Valley. The Johnson Valley Aquifer lies in the southeastern sections of the Este sub-basin, and extends east to Johnson Valley. As indicated earlier, both aquifers are being recharged through initial losses from infiltrating precipitation and transmission losses from ephemeral channels following precipitation events (Smith and Pimentel, 1998). In this study, we investigate a previously unrecognized additional source of recharge. Specifically, we investigate the potential role of the strike-slip faults in the basin as conduits for groundwater flow, providing recharge to both the local and regional aquifers. We also investigate the role of basement uplifts (ridges) in controlling lateral groundwater flow in the study area.

CHAPTER 2

METHODOLOGY

2.1 Methodology Overview

We adopted a four-fold methodology. Firstly, we collected and processed available satellite and airborne LIDAR images to better delineate the fault traces, as many of them are obscured by alluvium or too subtle to observe in the field. Secondly, we applied several geophysical techniques to verify the satellite-based distribution of faults using magnetic and electromagnetic measurements and to examine the role of faults and basement uplifts on groundwater flow. Thirdly, we collected groundwater samples from the study area to conduct isotopic analyses in search of isotopic provenances that are related to the distribution of faults and uplifts in the study area. Lastly, the collected geophysical and geochemical data were evaluated together with all other relevant hydrologic data (e.g., water levels, stream flow, and water chemistry) in a GIS environment for a better understanding of the spatial relationships.

2.2 Remote Sensing Methods

2.2.1 Light Detection and Ranging (LIDAR)

Airborne LIDAR utilizes a laser emission and detection system to send pulses of light (several hundred thousand per second) to the land surface, while measuring how long it takes to receive a backscatter signal

(<http://opentopo.sdsc.edu>). Through inertial tracking and real-time differential GPS, this process can be used to make extremely detailed digital elevation images of the surface, while stripping away surface obscurers such as vegetation, as seen in Haugerud et. al, (2003). Using densely packed laser emissions and detection apparatus, LIDAR images have the ability to return spatial resolutions on the order of 1 meter. This allows for small scale features, such as subtle topographic changes, and partially obscured small scale fault features to be easily observed and analyzed, where most other airborne and satellite datasets limited resolutions might cause them to be overlooked. This is ideal for areas like the Mojave, where even the large faults are often obscured or buried. Unlike ASTER, and IKONOS and other remote sensing data sets, LIDAR is not a satellite mounted imaging system and therefore is not a global data set. Due to the expense of equipment and mission flights, LIDAR datasets are generally unavailable for most areas of the country.

2.2.2 GeoEye-1

GeoEye-1 is a high resolution satellite launched by GeoEye (www.geoeye.com) in 2008. GeoEye-1 has a spatial resolution of 0.41m in the panchromatic band, and 1.65m for multispectral bands. All scenes are tonally balanced, map accurate, and pre-mosaicked, making them ideal for easily accessible and reviewable high resolution data. Scenes are available for more than 98% of the world, including the entire United States. The very high spatial resolution makes

these scenes ideal for examining smaller, less regional features such as fault splays and highly variable topography.

2.2.3 Advanced Spaceborne Thermal Emission and Reflection Radiometer (ASTER)

ASTER is an imaging instrument attached to the Terra Satellite, which was launched in 1999 as part of NASA's Earth Observing System (EOS) (www.asterweb.jpl.nasa.gov). The ASTER scenes with their 14 spectral bands in the visible, near-infrared, short-infrared and thermal infrared wavelength regions offer enhanced opportunities for lithologic mapping. Because the Helendale juxtaposes compositionally distinct rock units, the regional distribution of the fault traces were delineated from ASTER images processed in ways that enhanced compositional differences (Sultan et al, 1987). The ASTER scenes were used in conjunction with the LIDAR data to better map the regional extent of the Helendale Fault, and its subsequent splays and zones of deformation.

2.3 Geophysical Methods

2.3.1 Very Low Frequency (VLF) Profiles

The VLF band of the radio spectrum is between 3 kHz and 30 kHz. The Iris Instruments T-VLF Very Low Frequency Radio Receiver (WMU S/N 99) was used to measure the distortion of the normally horizontal electro-magnetic flux lines by local electrical conductors. It uses the radio carrier waves (15 – 30 kHz) of the submarine communications stations of the various navies of the world (Paterson and Ronka,

1971). This records for each frequency used, the tilt of the magnetic field (from the horizontal) given in percentage, the ellipticity in the vertical and horizontal planes, and signal strength.

The instrument has several limitations. It responds strongly to massive sulfides, as well as to graphitic shear zones; however the Mojave River Basin is not known to contain these types of sulfide deposits and shear zones, so it is unlikely that interference would present itself in this form. It is also limited to detection within an approximately 90 degree fan of strikes (± 45 degrees from the radial azimuth to the transmitting station). To combat this, measurements were recorded using one of three transmitting stations: Seattle (NLK at 24.8 kHz), which provided nearly ideal geometry for transects done in an east or northeast direction. Lamour, N. Dakota (NML at 25.2 kHz), which was available only for the 2011 data, was used for the northwest trending transects. Lastly, the Cutler, Maine (24.0 kHz) was used as an alternative, since the receiver collects from two stations simultaneously. Data from this frequency was generally only used for north trending transects. The VLF method is also limited to use during daylight hours, when the overhead ionosphere is well-developed (Vallee, et.al., 1992). It is also subject to sudden pulsations from the solar wind, which result in rapid deviations of the apparent tilt angle that may last for several minutes. In the event that unexpected or inexplicable anomalies were encountered, data collection would be paused or repeated to rule out this possible inference source.

Over the course of three summers (2009-2011), 25 transects were performed in various locations across or near to the Helendale fault (Fig. 3). These transects were most commonly taken in the exposed ridgelines along the southern portion of the Helendale, the lower alluvial portions of the valley, and the canyons in the northern portion of the Este sub-basin. Some of these transects were taken along suspected splays of the main fault, as opposed to crossing the Helendale Fault itself. Several of these splays were previously mapped, while others were identified using available geologic maps and remote sensing datasets. Seven of these transects will be detailed in the discussion section of this paper.

2.3.2 Magnetic Profiles

The Proton-Precession magnetometer (GeoMetrics G-816) was used to measure the absolute total magnetic field strength (in gammas or nanoTeslas [nT]) at the position of a sensor held on a staff approximately 2.5 meters above the ground. The total magnetic field, location, and time of acquisition were recorded for every station. Because the earth's magnetic field is subject to several time variations, the principal of which is the daily or diurnal variation, a profile is usually preceded with a reading (and time) at an arbitrary local base station (which may be the first station of the profile). The base station is then read again at the end of the transect. Since measurements along each of the transects were done in less than an hour, the drift could be approximated as a simple linear function and readily corrected. Of the 25

VLF profiles conducted, 18 had magnetic data collected simultaneously. Transects lacking magnetic data were due to unavailable or malfunctioning equipment. Of the seven profiles detailed in the discussion, five also have magnetic data.

2.3.3 Vertical Electrical Soundings

A vertical electrical sounding (VES) is a type of resistivity measurement that measures the electrical resistivity as a function of depth at a fixed point, assuming sub-horizontal layering (Telford, et al, 1990). The VES measurements taken in the field were performed using a 4-electrode expanding Schlumberger Array. In this array, the two measuring (or voltage) electrodes (M and N) are kept fixed for 3-5 different expansions of the current electrodes (A and B). Because the current electrode spacing (A-B) is the primary control of the depth distribution of current lines (in addition to the resistivity layering structure), the AB or AB/2 distance is the reference for each reading. We used AB/2 spacings that increased from 1.0 m to 147 m in equi-spaced intervals on a logarithmic scale, six spacings per decade. MN spacings were always 1/5 or less of the AB spacings. At the point where the measuring electrodes are expanded, another reading is taken without moving the current electrodes, which provides data overlap. In this way, any surficial, lateral resistivity changes near the measuring electrodes reveal themselves as a plot segment that is higher or lower than the adjacent segment(s). This can be corrected for by simply moving that segment up or down (multiplying by a constant, as this is a log plot), so that it matches the adjacent segment. Thus, the first stage of treatment of the

Schlumberger VES data is to make a smooth curve by either adjusting segments up or down, or if they show little offset (<1%) then simply averaging the overlap points is sufficient. A potential source for error in these measurements is based on the amplitude of the voltage reading. In the Mojave environment, when the voltage signal falls below about 2 milliVolts, the uncertainty of the calculated resistivity rises rapidly. Points that fell below this threshold have been rejected in this study. This method was the last field method implemented in this area, and was only conducted in the summer of 2011. A total of 10 VES stations were taken near a central location of the Helendale fault (Fig. 3)

2.4 Isotopic Methods

Two groups of water samples were collected and analyzed for their isotopic compositions (δD and $\delta^{18}O$). Twenty groundwater samples were collected (winter 2010) from shallow (depth: 35 to 40 m) production wells from the Old Woman Sandstone formation and six samples were collected (Spring 2011) from the springs at the foothills of the San Bernardino Mountains. H and O isotopic ratios in water were measured by standard methods of equilibration with H_2 and CO_2 respectively (Coplen, 1996; Nelson, 2000). Hydrogen and oxygen isotopes are reported in terms of the conventional delta (δ) notation, in units of per mil (‰) deviation relative to the Standard Mean Ocean Water (V-SMOW) and PeeDee Belemnite (PDB) standards (Coplen, 1996), where

$$\delta, \text{‰} = [(R_{\text{sample}} - R_{\text{std}})/R_{\text{std}}] \times 1000. \quad (1)$$

and $R = {}^2\text{H}/{}^1\text{H}$, or ${}^{18}\text{O}/{}^{16}\text{O}$. Reproducibility of δ values for δ D is $\pm 1\text{‰}$ and that of $\delta {}^{18}\text{O}$ is $\pm 0.2\text{‰}$. The samples were analyzed for the stable isotopes at ISOTECH Laboratories, Champaign, Illinois. Analysis of these isotopes can be used to determine the source(s) of groundwater and to identify mixing trends between these sources (e.g., Izbicki, 1998). In general, contrasts in these isotopic ratios across structural features such as uplifts and faults could be indicative of the role these features play as barriers to groundwater flow.

2.5 GIS Analyses

Analysis of the collected data for this project involved the generation of a database for data integration, analysis, and visualization. An Arc Info GIS environment was utilized for data manipulation and representation, using Arc Spatial Database Engine (SDE). All procedures and methodologies were adapted for use in this environment. The database incorporates all relevant co-registered digital mosaics with a unified projection (World Geodetic System [WGS] 84) covering the southern Mojave Desert: (1) Geologic Map (scale 1:250,000) (available at www.groundwater.fullerton.edu); (2) False-color mosaic of ASTER day scenes (spatial resolution 15m)(www.nasa.echo.gov) (3) 1.5 KM Light Detection and Ranging (LIDAR) swath (spatial resolution 1m) spanning the approximate length of the Helendale Fault (available via www.opentopo.sdsc.edu); (4) Well data including

one or more of the following parameters: well location, well name, well type (i.e. production, commercial, domestic, municipal), depth to water table, well elevation, and H and O stable isotopic compositions; (4) IKONOS and GeoEye-1 satellite scenes (spatial resolution 1-5m); (5) California Alquist-Priolo Earthquake Fault Zone maps (scale 1:24,000)(available via www.consrv.ca.gov); (6) vertical electrical sounding data from Lucerne Valley Bottom in the immediate vicinity of the Helendale Fault; (7) VLF and magnetic profiles acquired in tandem for dextral faults and intersecting fault splays in and near the Lucerne Valley and Helendale Fault areas.

CHAPTER 3

DATA AND DISCUSSIONS

3.1 VLF and Magnetic Data

If the hypothesis that the dextral faults and intersecting fault splays in the Lucerne Valley are channeling groundwater is plausible, a significant conductive response in the VLF would be expected as the transect crosses the fault plane. In cases where the fault plane is not readily apparent or well known, it is presumed that the magnetic signature of the underlying rock would show either a peak or trough indicating the presence of an area of changed magnetite content, such as those often encountered in zones of fault gouge, or an abrupt change in slope, indicating a juxtaposition of rock units of varying magnetic susceptibilities.

VLF data can be examined directly on tilt-angle *vs* transect distance plots. Conductors are located where the tilt angle changes sign, i.e. where there is a zero cross-over. Alternatively, simple filtering can be applied to remove short-wavelength features (e.g., single-station anomalies) and to shift the peaks by 90 degrees. The 4-point Fraser filter (Fraser, 1969) is widely used to accomplish this, and shifts the curve so that positive peaks are directly over the conductors. Note that Fraser used discrete station spacings of 50 ft. (15.24 m), as the typical wavelength of geologic anomalies due to a single sub-vertical conductor is about 150 ft. (45.7 m), or the horizontal distance subtended by the 4-station operator. The amplitude of peaks varies with distance from the transmitting station, average surface earth conductivity,

and time of day. Interfering noise depends on season, latitude, and solar activity, Thus, Fraser (1969) pointed out that in optimal conditions a filtered peak of 5 may be significant, and that values can go as high as 100. For this survey, we conservatively regarded Fraser-filtered peaks above 20 as significant, even though on some days the threshold could have been 10 or 15, as verified by comparing profiles repeated at the same location on different dates.

Figure 4 (a-c) show the VLF and magnetic transects at three locations (Fig. 3: T1104, T1103, T0209) along the northern portion of the Helendale Fault and its splays in areas proximal to the San Bernardino mountains. Scenes were re-oriented to display transects trending roughly left to right. The VLF and magnetic transect locations were plotted with colored circles, where hollow circles indicate a VLF response below a Fraser tilt of 0% (i.e., not conductive). A LIDAR swath or high resolution Geoeye-1 imagery was used as a background image and faults were mapped locally (dashed lines) from these images. Several scenes also have the California Alquist-Priolo (AP) fault zones as an added background. These zones outline buffer areas where risk of movement along active faults has been assessed since 1971 (www.consrv.ca.gov), as measured by the California Geological Survey. The VLF responses shown in figure 4 together with the magnetic measurements that were acquired simultaneously along the same transects were graphed figure 5. Similar displays (Fig. 6) and response graphs (Fig. 7) were generated for the VLF and magnetic transects (Fig. 3: T3001, T1003, T0105 and T1105) located along the

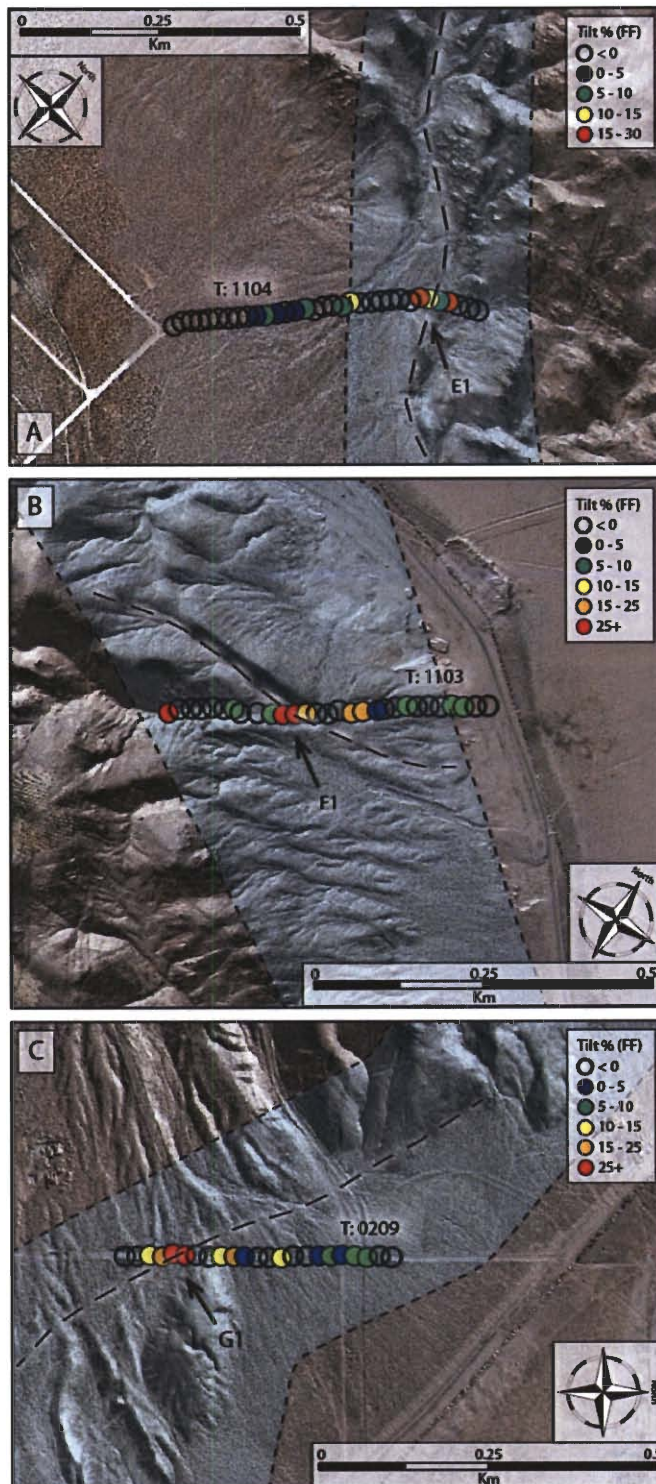


Figure 4. Selected VLF and Magnetic Transects for the northwest portion of the Helendale Fault. Fig. 4a-4c show strong VLF responses (Fraser Tilt %), where transects intersect the fault locations (dashed black line) within AP zones (light blue area outlined by black dotted lines). Figure 5d-f (located on the next page) shows the data plots (red lines: Fraser Tilt %; black lines: magnetic responses in nanoTeslas) for each of the measured transects. Appreciable VLF and magnetic responses (marked by arrows) correspond to known (black dashed lines) fault locations on Figs. 4a-4c.

northern portion of the Helendale fault, in the more mountainous region northwest of Lucerne Valley.

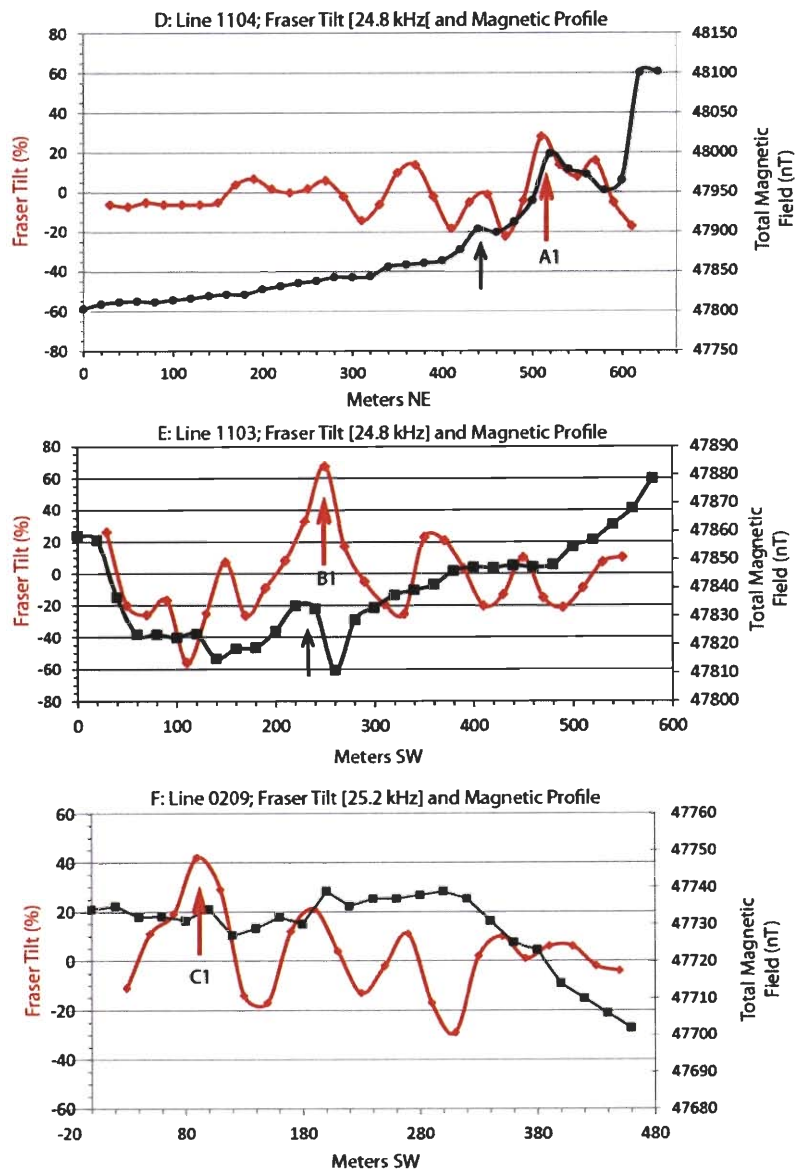


Figure 5. Corresponding VLF and magnetic plots for figure 4a-4c.

The following observations can be seen in figure 4. Transect 1104 was performed in a box canyon, moving west to east. The modest VLF peak (FT 30%) aligns well with the main trace of the Helendale Fault, which is well defined in the LIDAR dataset, and lies well within the mapped AP zone (outlined in light blue with thin black dotted lines). The magnetic response shows a change from sizable and short wavelength anomalies in the northeast to a smooth, gentle gradient in the southwest. This is clearly an indication of the juxtaposition of two different basement lithologies and/or shallow basement to the northeast and deeper basement to the southwest.

Transect 1103 shows good responses with both magnetic and VLF methods. The very strong VLF anomaly aligns with a clear dipolar magnetic response. Both responses align well with a mapped fault shown on the LIDAR image and is also identified on geologic maps. This fault also lies well within the mapped AP zone for the Helendale. This fault is most likely a branch of the primary Helendale that “kinks” through the large ridge, with the main trace being obscured to the east, or possibly still buried beneath the relatively shallow valley sediments. Another strong anomaly at the beginning of the profile aligns with another large fault, which is most likely responsible for creating the large depression seen in the LIDAR image.

Transect 0209 shows a strong VLF response (FT 45%) which aligns well with a mapped portion (AP zoning and local geologic maps) of the Helendale Fault, which

curves through the canyon in this area. The magnetic profile does not show any significant trend change or anomaly at this position.

Figure 6 (a-c) shows four VLF transects, two of which also have magnetic data, while figures 7 (d-g) shows the VLF and magnetic data plots for these transects. Transects 3001 and 1003 (T: 3001, T: 1003) are repeat transects, done each year in the same approximate location. T: 1003 was performed in summer of 2009 while T: 3001 was performed in summer of 2011. T: 3001 shows a single, well defined peak with a Fraser tilt of 45% very near the fault plane, while T: 1003 shows a similar peak with a tilt of 58%. Both peaks align very well with the mapped AP zone for this area of the Helendale Fault as well. While not shown, this was also the case in the repeat transect from 2010. The profile from 2011 showed a significantly higher response than that of 2009 and 2010 (15-25% higher). This is most likely due to the timing of the profile and the increased amount of groundwater still present in the fault plane when measured. Transects performed in 2011 were conducted much earlier in the season than those in 2009 and 2010. Additionally, 2011 was a wet year by comparison to 2009 and 2010. Both factors would lead to a higher amount of groundwater and therefore a stronger response. Transect 0105 runs parallel to the Helendale Fault and crosses at high angles a series of suspected fault splays which intersect the Helendale itself. In each case an appreciable peak (FT 20% or greater) is seen as the transect crosses the fault trace, indicating the presence of shallow subvertical conductive sheet, most likely groundwater within high-angle fault splays.

If these splays connect to the Helendale, they can possibly collect additional groundwater to add to that already channeled by the main fault. The magnetic profile shows a much larger range of variability than most other transects measured on this project. There were obvious lithology changes along the profile and some of the abrupt magnetic changes are most likely due to this. Transect 1105 crosses a suspected splay of the Helendale (Helendale is mapped as a black, dashed line) in the far south, which splits into two small subsplays (mapped as red, dashed lines). The fault traces here are fairly well defined, and two appreciable VLF peaks are observed as each fault trace is crossed, again indicating the presence of a shallow, conductive material. The magnetic profile for this transect is quite varied, showing an abrupt change in slope as each fault trace is crossed. This is observed particularly well at location B2.

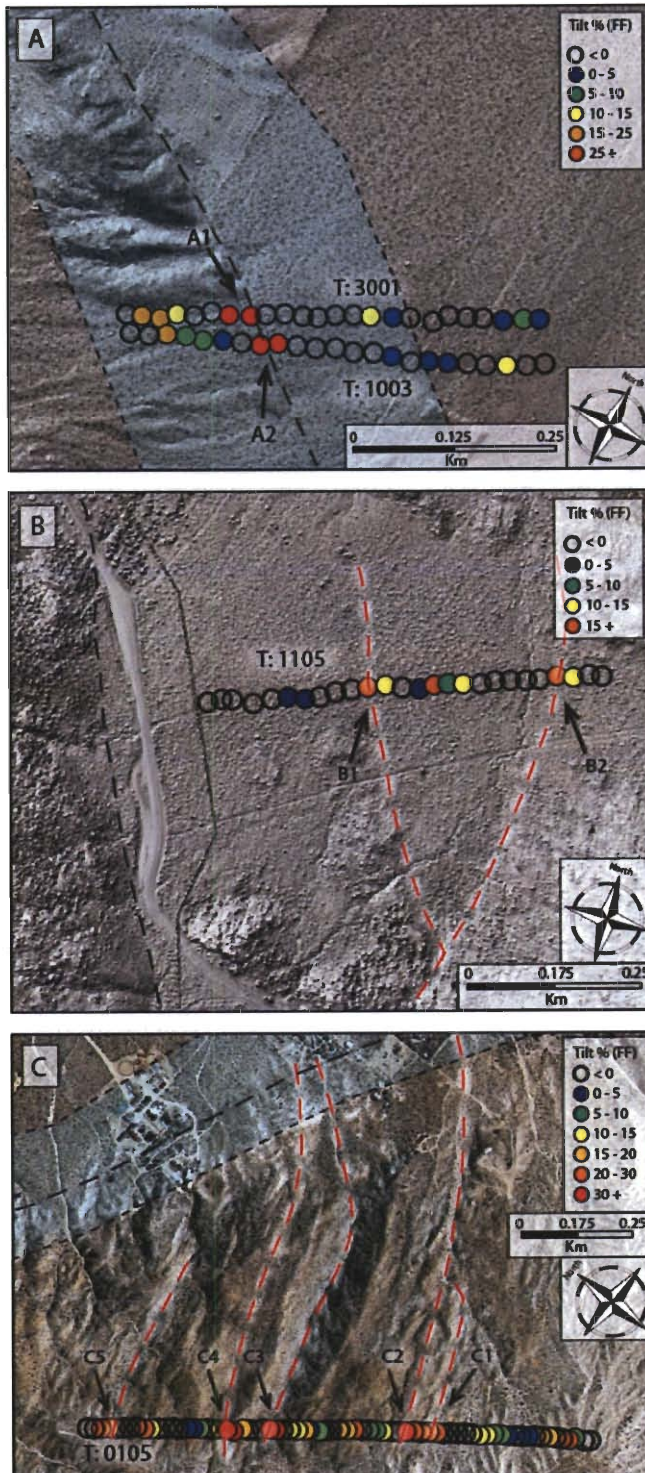


Figure 6. Selected VLF and magnetic transects for the southeast portion of the Helendale (black dashed line) Fault. Fault splays (red dashed line) were mapped from LIDAR and Geoeye-1 imagery, and AP zones are applied where applicable (light blue area outlined by black dotted lines). (6a-6c) show very strong VLF responses. (7d-7g, located on page 27) show the data plots (red lines: Fraser Tilt %; black lines: magnetic responses in nT) for each of the measured transects. Appreciable responses (marked by arrows) correspond to known fault locations (black dashed lines) or LIDAR and satellite-based inferred fault locations (red dashed lines) on Figs 6d-g.

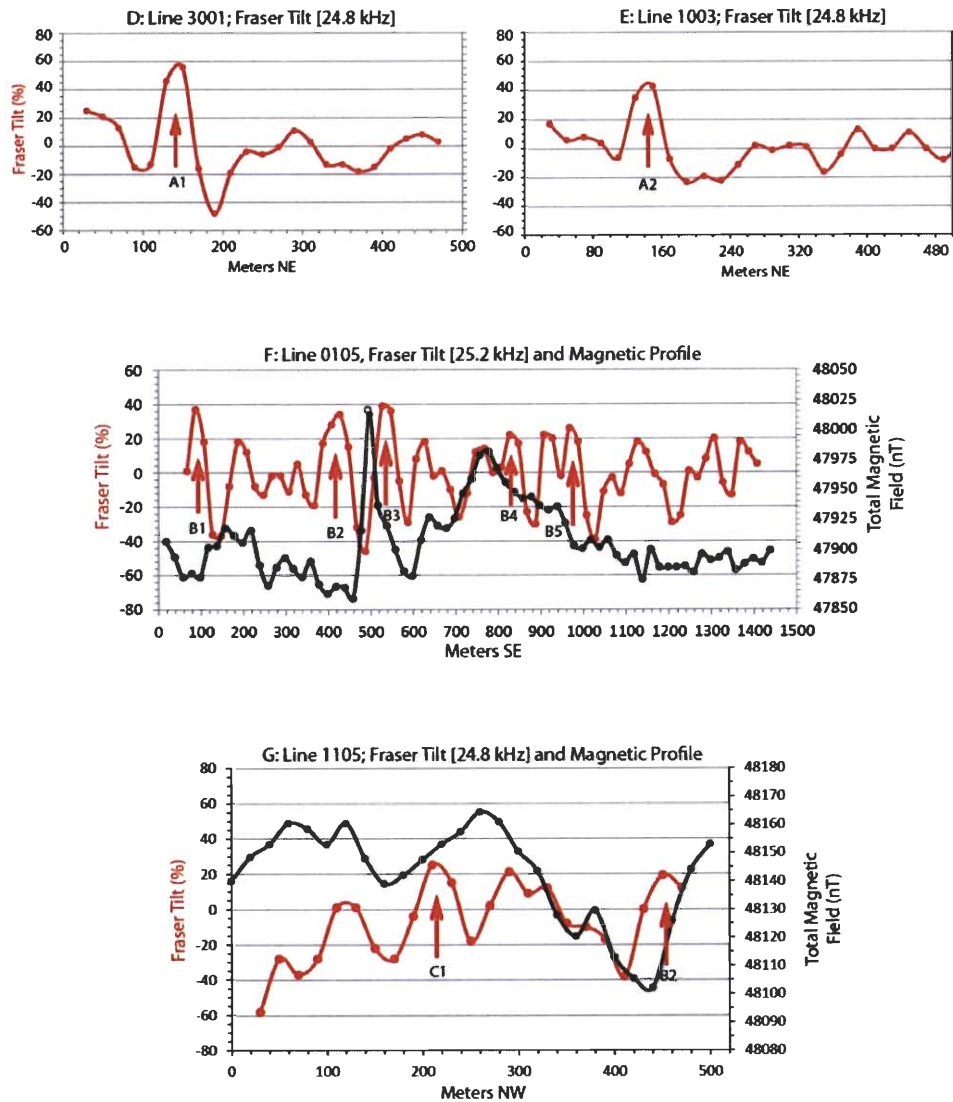


Figure 7. Corresponding VLF and magnetic plots for figure 6d-6g.

3.2 VES Data

The ten Schlumberger VES sounding locations and the location of the single multi-level Electrical Resistivity (ER) transect are shown on Fig. 8. The 8 VES's near the fault were expanded in the NNW sense, parallel to the fault, or NS along

roads (VES's 4 and 9). VES 9, 4, 6 and 7 were run parallel to the E side of the fault, VES 10, 1, 5, and 8 were run parallel to the W side of the fault. Additionally, soundings 2 and 3 were performed west of VES 1. This row (3, 2, 1 and 4 respectively) of soundings shows how the subsurface characteristics change across the fault.

East of the fault, the four soundings show a strong similarity in curve types, all with two maxima. The northernmost sounding (VES 9) shows the first maximum is at the surface and becomes progressively deeper to the south. The intervening minimum and the second maximum also become progressively deeper (move to the right on the VES plot) and overall resistivities increase as the soundings progress SSE and up the alluvial fan to higher elevations. Each of these four soundings ends with a steeply declining branch, indicating that the conductive, saturated zone is being detected. It should also be noted that this conductive zone is observed at deeper and deeper depths to the south-southeast. The two maxima are likely coarse grained vadose zone sediments, sandwiching a more conductive fine-grained unit.

A greatly differing trend is observed west of the fault. In general, a much lower trend in resistivities is observed in each of the soundings when compared to similarly placed soundings east of the fault. They are similar in that the resistivities rise moving north to south, up the alluvial fan surface. The right (deepest) branch of the log-log VES curves 1, 5 and 8 show an increase in resistivity. This is contrary to the case on the east side of the fault, and the most plausible interpretation is that

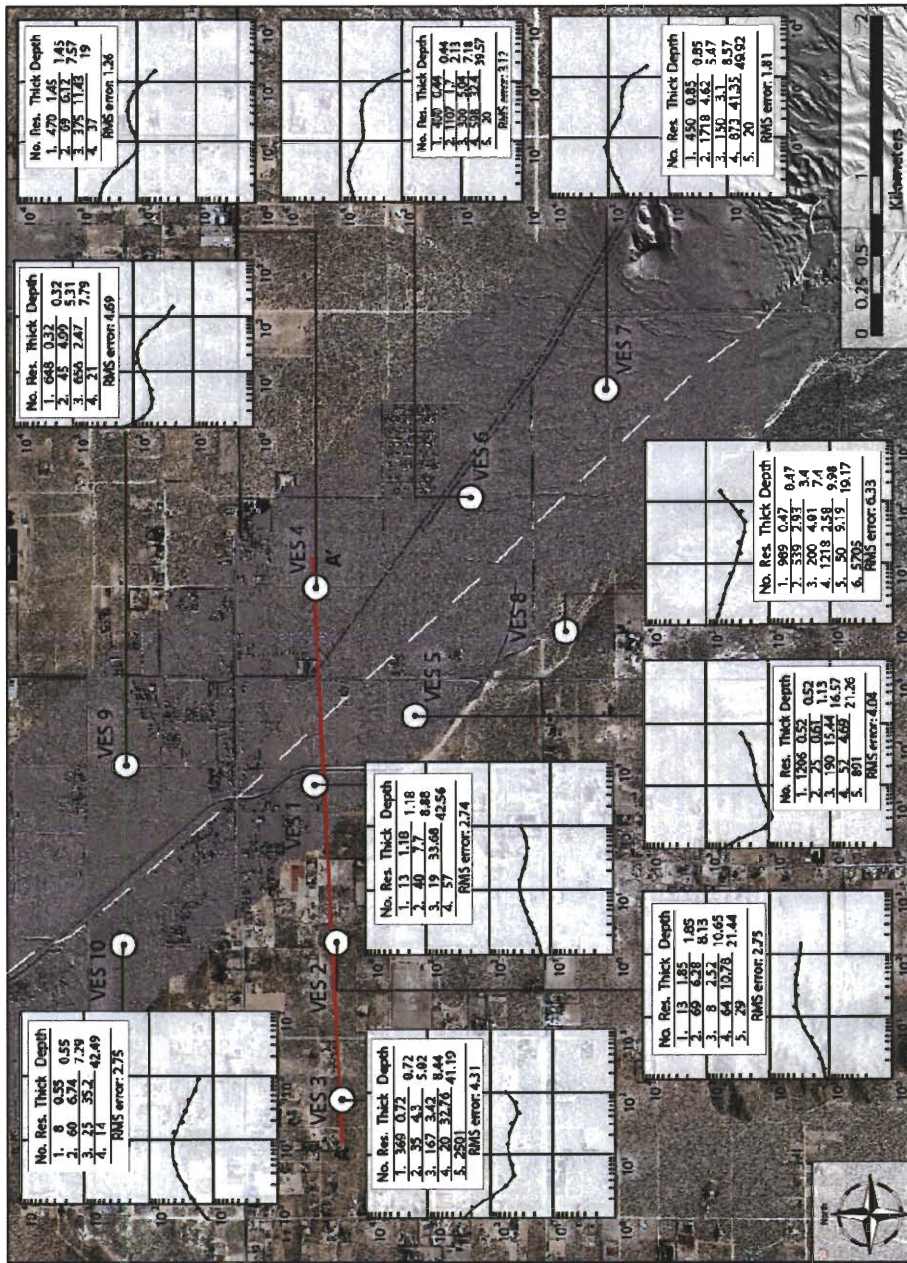


Figure 8. VES Location, apparent resistivity, thickness, and distribution of saturated and unsaturated rock units in areas west (VES 10, 3, 2, 1, 5 and 8) and east (9, 4, 6 and 7) of the Helendale Fault (white dashed line).

bedrock has been encountered at fairly shallow depths. These sections were conducted along the strike of the topographic ridge to the southeast (Boxes C and D in Fig. 3 are conducted along this ridge), and would appear to make a strong case for the continuation of that bedrock ridge in the subsurface all the way north to Lucerne Valley. If this is the case, then this bedrock ridge just to the west of the Helendale fault is likely what is blocking eastward flow of groundwater across the fault. Flow is then only possible through a passage on the order of one mile wide at the valley bottom, starting north of VES 1 and terminating against a ridge slightly north of VES 10 (this is the same ridge seen in Fig.2a, and also in Fig. 3 where the transects seen in Box B were performed).

Soundings 3, 2, 1 and 4, which were performed in a row crossing the fault east to west, show a clear change across the fault between soundings 1 and 4. It also shows the low resistivity of the two central soundings (VES 2 and VES 1) where the surface sediments consisted of fine silts and clays, typical of the valley floor. The surface material at VES 3 was coarser, which typically shows higher resistivity, but the deeper resistivities were also low, as with soundings 1 and 2. The deepest segment of the curve for sounding 3 is a rising branch, possibly indicating another area of shallow bedrock. Another, much smaller ridge is seen to the southeast of sounding 3, and appears to continue to the northwest. It is reasonable to assume that this ridge, like the ridge that parallels the Helendale Fault, simply extends into the shallow subsurface before outcropping again to the northwest.

When the inversion outputs for a row of VES's are taken and plotted as a cross section showing boundaries between layers and the layer resistivities added, the result can be displayed as a 2-D geoelectrical section. At that point, zones of similar resistivities can be correlated as in a fence diagram between wells, except that in this case it is the VES solutions (resistivity vs depth) rather than wells that are being correlated. A diagram of this sort was made in the W-E direction to show the changes across the fault (Fig. 9). Line A-A' shows that the vertical resistivity structure at VES#4 is totally different from that of VES's 1-3. West of the fault, the water table is interpreted at about 7-10 m depth, and a short distance east of the fault it is double that value. Also to the east a thick, high-resistivity (375 Ohm-m) unsaturated zone is present, while to the west it is much lower resistivity, probably reflecting finer-grained sediments. Two of the VES's to the west appear to have reached high-resistivity basement rock at depths of about 40 m. This supports the hypothesis of a shallow bedrock sill joining the topographic ridges to the NW and SE. The eastern limit of this sill would be the Helendale Fault, and the western limit would be the beginning of the deeper Fifteen Mile Aquifer about 3 kilometers west of the Helendale Fault.

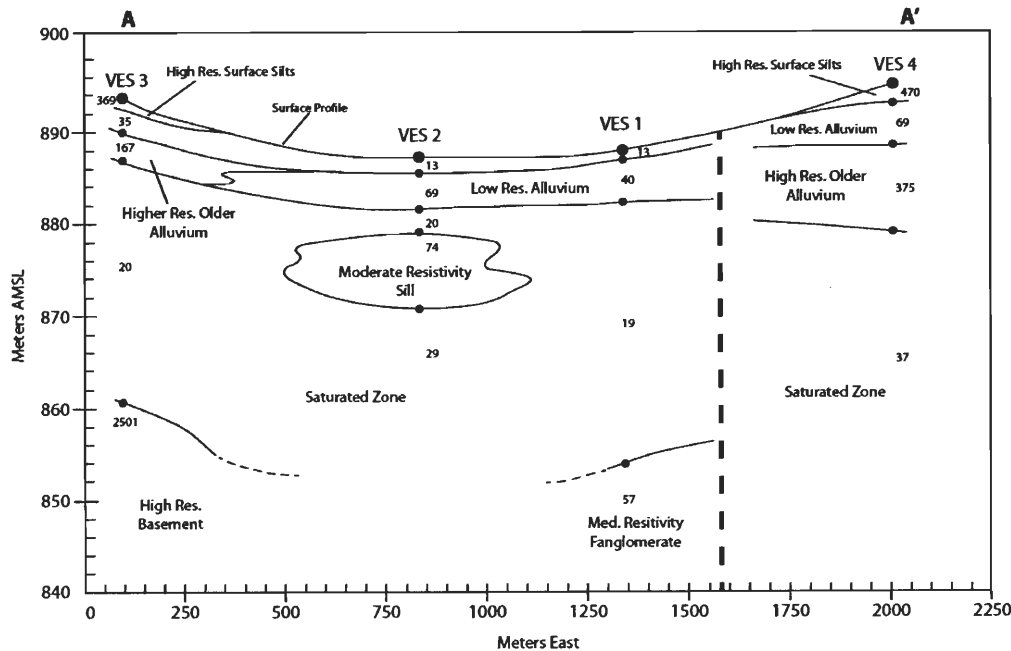


Figure 9. Geoelectric Cross Section along line A-A' shown in figure 8. Line shows geoelectrical layering differences from west to east across the fault: apparent resistivity values in Ohm-m.

3.3 Isotope Data

Isotopic analyses (δD and $\delta^{18}O$) were conducted on groundwater samples collected (fall 2010) from productive wells and springs sampled in summer of 2011. The distribution of the well and spring samples is given Fig. 10 and the isotopic analyses of these samples are presented in Table 1 and Fig. 11; well and spring samples are labeled as “mwa” and “wmu” samples, respectively. Inspection of Table 1 and Figs. 10 and 11 shows that the samples to the west of the fault (mwa: 1,2,11,13-16; wmu: 1,2,3) from the Lucerne Valley Aquifer and proximal to the fault (mwa: 1,12,13,14,19; wmu: 3,5,6), hereafter referred to as group I samples, have depleted

isotopic compositions (δD : -84.7 to -94.1; $\delta^{18}O$: -10.54 to -12.61‰; Average δD : -88.1 ‰) and plot along an evaporation line (Fig. 9; EVL1), an observation that is consistent with a unified source (S1) whose composition (δD : -88; $\delta^{18}O$ -12.3) is given by the intersection of the evaporation and global meteoric lines. Because a number of these samples were collected from springs (wmu: 1, 2, 3, and 5) at the foothills of the San Bernardino Mountains, we suggest that the source of group I samples is largely the melt of the snow falling over the mountains. This suggestion is consistent with earlier findings (USGS, 2004) that suggest that the Regional Aquifer is being recharged by runoff and groundwater flow from the San Bernardino Mountains in the south.

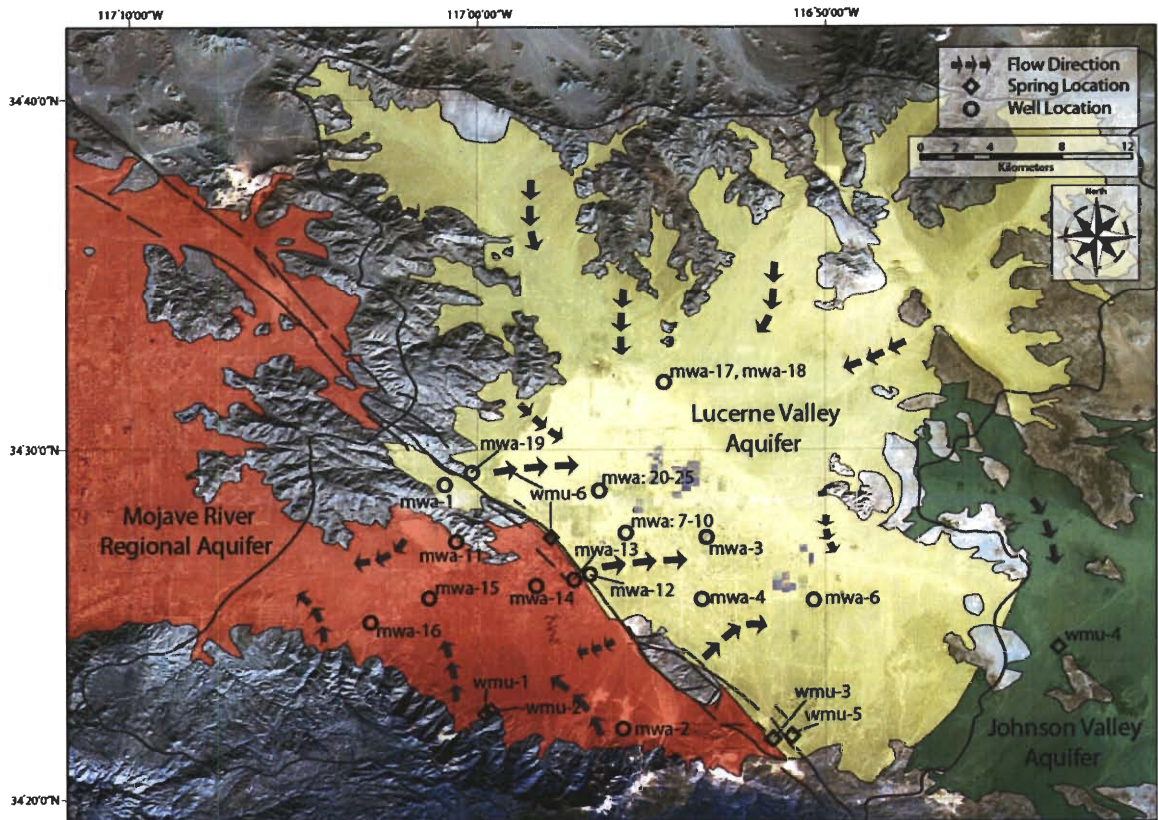


Figure 10. Locations of wells (open circle; name designation: mwa) and springs (open diamond; name designation: wmu) sampled for isotopic analyses (O, H). Also shown are: (a) principal aquifers including Regional Aquifer (red area), Lucerne Valley Aquifer (yellow area), and Johnson Valley Aquifer (green area), (b) groundwater flow direction indicated by arrows, and (c) the Helendale Fault (modified from ESA, 2004; Stamos et al, 2001, 2004).

Table 1. List of well and spring samples, including naming schema, specific and general location information, elevation, and isotope data. Well type and sample depth are also included where applicable.

Sample ID	Name	Aquifer	Latitude	Longitude	Elevation (fa.s.l.)	Description	Sample Depth (ft)	DWT (ft)	δD ‰	$\delta^{18}O$ ‰
219848	wmu-1	Regional Aquifer	34.37575	-116.9929	4449	Mountain Front Spring	N/A	0	-85.6	-11.8
219849	wmu-2	Regional Aquifer	34.37468	-116.9945	4449	Mountain Front Spring	N/A	0	-85.2	-11.4
219850	wmu-3	Lucerne Valley	34.36283	-116.8575	4589	Mountain Front Spring	N/A	0	-88.3	-11.7
219851	wmu-4	Johnson Valley	34.40575	-116.7208	3172	Valley Spring	N/A	0	-96.6	-12.5
219852	wmu-5	Lucerne Valley	34.36406	-116.7488	4167	Mountain Front Spring	N/A	0	-86.5	-10.4
219853	wmu-6	Regional Aquifer	34.45823	-116.9636	2871	Valley Spring	N/A	0	-84.7	-10.5
03N01W12A01	mwa-2	Regional Aquifer	34.3669	-116.9295	4145	Production Well	-	-	-87.5	-11.6
04N01E09D04	mwa-3	Lucerne Valley	34.45752	-116.8893	2926	Production Well	-	-	-91.6	-12.2
04N01E16N02	mwa-4	Lucerne Valley	34.42977	-116.891	3037	Domestic Well	225	165	-93.2	-12.2
04N01E21A02	mwa-5	Unknown				Domestic Well	-	-	-90.7	-12.3
04N01E24D03	mwa-6	Lucerne Valley	34.42797	-116.8384	3063	Domestic Well	-	-	-91.8	-11.9
04N01W01R04	mwa-7	Lucerne Valley	34.46049	-116.9283	2877	Municipal Well	180	155	-97.5	-11.6
04N01W01R05	mwa-8	Lucerne Valley	34.46049	-116.9283	2877	Municipal Well	180	152	-100.7	-12.8
04N01W01R07	mwa-9	Lucerne Valley	34.46049	-116.9283	2877	Municipal Well	143	136	-92.0	-12.1
04N01W01R08	mwa-10	Lucerne Valley	34.46055	-116.9283	2877	Municipal Well	180	153	-91.8	-12.5
04N01W13D01	mwa-12	Lucerne Valley	34.44022	-116.9456	2967	Commercial Well	-	-	-91.2	-12.3
04N01W14G03	mwa-13	Regional Aquifer	34.438	-116.952	2967	Domestic Well	-	-	-91.4	-12.4
04N01W15K04	mwa-14	Regional Aquifer	34.43518	-116.9714	3008	Domestic Well	-	-	-88.2	-12.2
04N01W18Q01	mwa-15	Regional Aquifer	34.42903	-117.0219	2985	Municipal Well	165	83	-87.9	-11.9
04N02W24M01	mwa-16	Regional Aquifer	34.417	-117.05	3390	Domestic Well	-	-	-86.4	-11.7
05N01E08N03	mwa-17	Lucerne Valley	34.53181	-116.9104	2880	Municipal Well	180	152	-95.6	-10.5
05N01E08N04	mwa-18	Lucerne Valley	34.53181	-116.9104	2880	Municipal Well	180	152	-97.7	-11.0
05N01W29H02	mwa-19	Lucerne Valley	34.489	-117.002	2902	Domestic Well	-	-	-94.1	-12.6
05N01W32E01	mwa-1	Lucerne Valley	34.483	-117.015	3007	Domestic Well	-	-	-85.3	-11.0
05N01W36F01	mwa-20	Lucerne Valley	34.48049	-116.9405	2854	Municipal Well	143	128	-96.7	-11.8
05N01W36F02	mwa-21	Lucerne Valley	34.48049	-116.9405	2854	Municipal Well	145	129	-98.3	-12.4
05N01W36F03	mwa-22	Lucerne Valley	34.48049	-116.9405	2854	Municipal Well	175	128	-93.9	-12.4
05N01W36F04	mwa-23	Lucerne Valley	34.48049	-116.9405	2854	Municipal Well	175	129	-93.3	-12.8
05N01W36F05	mwa-24	Lucerne Valley	34.48049	-116.9405	2854	Municipal Well	125	105	-94.3	-12.8

Samples collected east of the fault, from the Lucerne Valley Aquifer, hereafter referred to as Group II samples, are generally more depleted compared to Group I samples. It is likely that the Lucerne Valley Aquifer is recharged largely from precipitation over the northern mountains (Ord, Rodman, and Stoddard mountains) (Blazevic, 2007). The groundwater flow in the Lucerne Valley is towards the southeast (Fig. 10). We speculate that the depleted nature of group II samples (Lucerne Valley Aquifer) compared to Group I (Regional Aquifer) could be related to compositions that are dominated by fossil groundwater that was precipitated in

previous wet cool climatic conditions in the case of Group II samples as opposed to the less depleted modern precipitation that are being precipitated in relatively warmer conditions (USGS 2004) prevailing nowadays. This suggestion is supported by the fact that the precipitation over the source areas (San Bernardino mountains) for the Regional Aquifer far exceeds that for the source areas (Newberry and Ord mountains) for the Lucerne Valley Aquifer (Izbicki 2004, USGS 2004). This can potentially lead to excessive flushing of the fossil water in the Regional Aquifer, and less of it in case of the Lucerne Valley Aquifer.

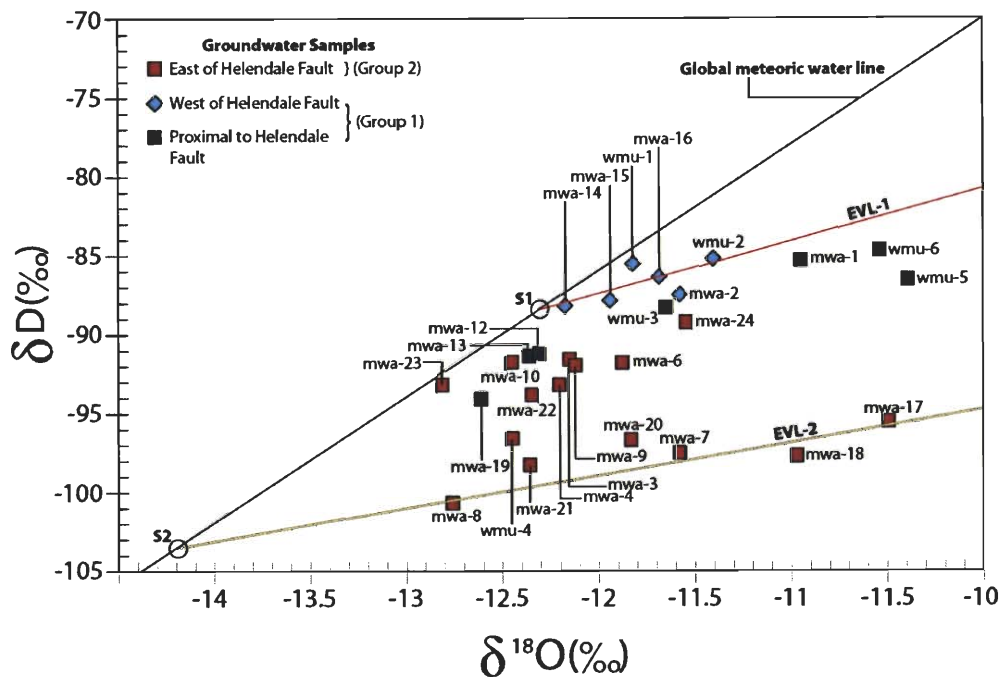


Figure 11. Comparison between stable isotope ratios [hydrogen (δD) vs oxygen ($\delta^{18}O$)] for groundwater samples from wells and springs west, east, and proximal to the Helendale Fault. Also shown are the evaporation lines EVL1 And EVL2, for Group I and Group II samples, respectively and their intersections (S1 and S2) with the Global Meteoric Line ($\delta D = \delta^{18}O + 10$; Craig, 1961). Arrows represent groundwater flow directions (ESA, 2004; Laton, 2005) for the major aquifers.

Group II samples show a wide range of variation in their isotopic composition (δD : -85.30 to -100.7; $\delta^{18}\text{O}$: -10.39 to -12.81‰; Average δD : -93.6‰) compared to group I samples. The most depleted of these samples (mwa: 7, 8, 17, 18) plot along an evaporation line (Fig. 11; line EVL2) that defines a source (S2) with an isotopic composition of δD : -104; $\delta^{18}\text{O}$ -14.2 at its intersection with the global meteoric line. The remaining Group II samples plot towards the compositions of group I samples. The isotopic composition of these samples is consistent with an explanation that calls on various degrees of mixing between two sources (S1 and S2) and various degrees of evaporation for each of the two sources and samples.

Several samples were taken from areas on either side of the Helendale Fault, in relatively close proximity to each other (mwa-13 and mwa-12; wmu-3 and wmu-5). In each case, the samples plot along the upper evaporation line, indicating their composition is that of Group I. This observation is consistent with the interpretation that the Helendale is actively channeling groundwater along its length from the San Bernardino Mountains.

It is commonly thought that the Helendale Fault acts as a barrier to lateral groundwater flow (Stamos et al, 2001; ESA, 2004; Smith and Pimentel, 1998) which would prevent groundwater from the Fifteen Mile Valley Aquifer from mixing with that of the Lucerne Valley Aquifer. This does not appear to be the case. Several water samples have δD and $\delta^{18}\text{O}$ values which plot between the two principal

evaporation lines for these waters (Fig 11). These wells typically are those east of the Helendale Fault, and fall along the east-southeast flow path of the Lucerne Valley groundwater. This indicates that mixing of groundwater is occurring within the Lucerne Valley Aquifer. This would make sense if there are open “windows” between the shallow bedrock ridges that trend along the fault across which groundwater is able to flow. Two of these windows, where groundwater flow appears to be uninhibited, occur in the vicinity of wells mwa-13 and mwa-12, as well as at springs wmu-3 and wmu-5. In each case, the bedrock ridge that cuts across the majority of the valley floor is unexposed at the surface. Since water levels west of the fault are relatively shallow, it is plausible that water is able to spill over the bedrock barrier in these locations, facilitating mixing between the aquifers. It is also likely that the fault itself is helping facilitate this mixing, as groundwater channeled through the fracture planes along the bedrock ridges would also spill into the aquifers along the valley floor as these ridges dip into the subsurface below the overlying alluvium. Regardless of which hypothesis is adopted, groundwater samples from the Lucerne Valley Aquifer that have mixed isotopic compositions must have been derived, at least in part, from recharge waters in areas west of the fault because if an impermeable barrier were preventing lateral flow, these anomalous mixed composition values could not be explained.

CHAPTER 4

SUMMARY

4.1 Interpretation of Results

There are differing camps when it comes to the Helendale Fault and how it interacts with the groundwater aquifers it intersects. The commonly accepted opinion is that the fault (and other faults in this area) is a barrier to groundwater flow, and is thus responsible for the observed local differences in water level across the fault (Stamos et al., 2003). This, potentially, has many implications for future water supply for the High Desert, as pumping of these aquifers can and will be heavily influenced by availability of water as well as sustainability of the aquifers through recharge. If the faults are preventing the movement of groundwater, recharge for those aquifers may be limited on either side, making sustainable water supply a non-option. It is likely that the fault itself is not what is preventing groundwater flow, but rather the surface and subsurface geology. Fluid transport through fractured and faulted crystalline rocks and the role of fault zone architecture and related permeability as the primary controls on fluid flow in brittle fault zones has been discussed (Barton et al., 1995; Caine et al., 1996; Evans et al., 1997; Gudmundsson, 2001; Sultan et al., 2007). For example, it has been demonstrated that the Najd Shear System, a complex of brittle faults and shear zones in the Arabian-Nubian Shield, and the largest transcurrent Pre-Mesozoic fault system on Earth acts as a conduit for groundwater flow, allowing significant amounts of groundwater to be channeled to

areas normally outside the reach of standard recharge and groundwater inflow (Sultan, 2007).

The VLF data has shown that the majority of locations along the Helendale Fault are conductive, indicating that the fault plane contains groundwater, even at higher elevations on the southern ridges. It is likely that the Helendale Fault is acting as a conduit for groundwater flow, channeling groundwater from the higher elevation areas in the south to the lowland areas in the central and northern portions of the Mojave River Basin. Magnetic data generally indicates an abrupt change in magnetic composition across the fault, which suggests a juxtaposition of units with varying magnetic susceptibilities. This is to be expected as shallow basement ridges are generally observed west of the fault, while dry lake and playa sediments are typically observed east of the fault.

The isotopic data is also consistent with the Helendale acting as a conduit. Two main groups of groundwater samples were found in the study area based on their distribution and isotopic compositions: (1) Group I were sampled from the Mojave River Regional Aquifer west of the fault and are compositionally less depleted than samples collected from the Lucerne Valley Aquifer east of the Fault (Group II). Groups I and II samples show evidence for varying degrees of evaporation. Several samples were taken from wells proximal to the Helendale Fault, typically from areas east of the Helendale Fault, along the east-southeast flow path of the Lucerne Valley groundwater. These samples plot along, or close to, the upper evaporation line,

indicating that their composition is largely that of Group I sample, the San Bernardino Mountain recharge waters, but show evidence for mixing with the Group II waters, the Lucerne Valley groundwater. One way for such mixing to occur is for the fault to channel groundwater through its fracture planes, many of which are observed within the bedrock ridges, as these ridges dip into the subsurface below the overlying alluvium. If the Helendale fault acted as an impermeable barrier preventing lateral flow, these anomalous mixed composition values from the Lucerne Valley Aquifer could not be explained, as these samples must have been derived, at least in part, from recharge waters in areas west of the fault.

If the Helendale is not a barrier for lateral groundwater flow, then what is causing the observed change in water level across the fault? West of the fault, groundwater is found an average of 5-10 m below surface level, while to the east of the fault; groundwater averages 45 m below surface level (Stamos et. al., 2003; Smith and Pimentel 1998). Our geophysical data (VES's) suggest that the groundwater drop across the Helendale can be attributed, at least partially, to the shallow bedrock ridges which prevent the groundwater from flowing eastward across the fault.

West of the fault, high resistivities are observed occurring at greater sounding depths, which is characteristic of shallow bedrock. These high resistivities occur along strike of a prominent bedrock ridge, which runs parallel to the Helendale Fault, and dips below the surface along the valley floor. It is likely that these resistivity highs are simply the continuation of this bedrock ridge. Further west of the fault,

shallow resistivity is much lower, and fits with mapped geologic units of young alluvium overlying older, higher resistivity alluvium. Further west still, another deep resistivity high is seen, again along strike of a bedrock ridge to the southeast. It is quite possible that these ridges are preventing groundwater from flowing eastward through the faulted zone.

4.2 Regional Implications

Results indicate that the Helendale and intersecting fault splays are acting as conduits for groundwater flow and are able to actively channel groundwater from the higher precipitation mountains in the southeast, to the lower portions of the valley to the north and northwest. This is evidenced by the conductive responses observed in the VLF data, and via the mixed isotopic compositions found in close proximity to the fault. Resistivity also suggests that lateral flow across the fault is indeed possible, and that the fault is not acting as a total barrier to flow. This is also evidenced by the isotopic compositions of the aquifers proximal to the fault. This study highlights the potential for identifying similar zones throughout the Mojave Desert Region, as it is likely that similar faults, especially those with exposed bedrock ridges trending along their length (Lenwood, Camp Rock, Calico, Granite Mountains, and Johnson Valley faults) will exhibit similar behavior. From a groundwater supply standpoint, this is of great importance, as it indicates additional resources may be available for the dry, low precipitation areas which are increasing in population each year.

REFERENCES

- Barton, C.A., Zoback, M.D., Moos, D., 1995, Fluid-flow along potentially active faults in crystalline rock: *Geology*, v. 23, no.8, p. 683–686.
- Blazevic, M., Laton, W.R., Foster, J., 2008, Geologic Insight to Lucerne Valley Groundwater Basin [Thesis Related Publication]: California State University Fullerton, 5 p.
- Caine, J.S., Evans, J.P., Forster, C.B., 1996, Fault zone architecture and permeability structure: *Geology*, v. 24, no. 11 p. 1025–1028.
- Coplen, T.P., 1996. New guidelines for reporting stable hydrogen, carbon, and oxygen isotope-ratio data: *Geochimica et Cosmochimica Acta*, vol. 60, Issue 17, p. 3359–3360.
- Dailey, D., Sauck. W., Mohammed, S., Milewski, A., Laton, W.R., Foster, J., 2010, Transcurrent Fault Systems in the Mojave Desert, Conduits or Barriers to Groundwater Flow?, *in* AGU National Meeting, San Francisco, California, November 2010.
- Dokka, R., 1983, Displacements on late Cenozoic strike-slip faults of the Central Mojave Desert, California: *Geology*, v. 11, no. 5 p. 305-308.
- Dokka, R., Travis, C., 1990, Late Cenozoic Strike-Slip Faulting in the Mojave Desert, California: *Tectonics*, Vol. 9, No. 2, p. 311-340.

- Dokka, R., Macaluso, Y., 2001, Topographic effects of the Eastern California Shear Zone in the Mojave Desert: *Journal of Geophysical Research*, Vol. 106, No. 12, p. 30625-20644.
- Environmental Science Associates (ESA) 2004, Mojave Water Agency 2004
Regional Water Management Plan: Program Environmental Impact Report,
SCH#: 2003101119.
- Evans, J.P., Forster, C.B., Goddard, J.V., 1997, Permeability of fault-related rocks, and implications for hydraulic structure of fault zones: *Journal of Structural Geology*, vol. 19, issue 11, p. 1393–1404.
- Fraser, D.C., 1969, Contouring of VLF-EM data: *Geophysics*, Vol. 34, No. 6, p. 958-967.
- Garfunkel, Z., 1974, Model for the late Cenozoic tectonic history of the Mojave Desert, California and for its relation to adjacent areas: *Geological Society of America Bulletin*, v. 85, p. 1931-1944.
- Geothermal Surveys, Inc. (GSI), 2000, Results of Detailed Gravimetric Investigation, Yucca Mesa Area, San Bernardino County, California: Prepared for High Desert Water District. June 12, 2000.
- Gonfiantini, R. (1978). Standards for stable isotope measurements in natural Compounds: *Nature*, vol. 271, p. 534-536.
- Gudmundsson, A., 2001, Fluid overpressure and flow in fault zones: field measurements and models: *Tectonophysics*, vol. 336, p. 183–197.

- Haugerud, R., Harding D., Johnson, S., Harless, J., Weaver, C., 2003, High-Resolution Lidar Topography of the Puget Lowland, Washington: GSA Today, Vol.13, No.6, p. 4-10.
- Izbicki, J., Danskn, W., Mendez, G., 1998, Chemistry and Isotopic Composition of Ground Water Along a Section Near the Newmark Area, San Bernardino County, California: USGS Water-Resources Investigations Report 97-4179
- Izbicki, J., Michel, R., 2004, Movement and Age of Ground Water in the Western Part of the Mojave Desert, Southern California, USA: USGS Water-Resources Investigations Report 03-4314
- Izbicki, J., 2004, Source and Movement of Ground Water in the Western Part of the Mojave Desert, Southern California, USA: USGS Water-Resources Investigations Report 03-4313
- Kennedy/Jenks/Todd LLC, 2007, Basin Conceptual Model and Assessment of Water Supply and Demand for the Ames Valley, Johnson Valley, and Means Valley Groundwater Basins: Contracted Report, Prepared for Bighorn Desert View Water Agency and Mojave Water Agency.
- Laton, W.R., Foster, J., Blazevic, M., Napoli, N., Perez, R., 2005, Este Hydrologic Sub-Basin Hydrogeologic Report: Prepared for and Submitted to Mojave Water Agency, California State University, Fullerton Department of Geological Sciences.

- Lewis, R.E., 1972, Ground-water Resources of the Yucca Valley-Joshua Tree Area, San Bernardino County, California: USGS Open-File Report 72-234, 51 p.
- NASA California Institute of Technology, Ongoing, www.asterweb.jpl.nasa.gov, open resource for ASTER datasets and bibliography (August 2010).
- Nelson, S.T., 2000. A simple, practical methodology for routine VSMOW/SLAP normalization of water samples analyzed by continuous flow methods: Rapid Communications In Mass Spectrometry, vol. 14, p. 1044-1046.
- Palacky, G.J., Ritsema, I.L. and De Jong, S.J., 1981, Electromagnetic Prospecting for Groundwater in Precambrian Terrain in the Republic of Upper Volta: Geophysical Prospecting, Vol. 29, p. 932-955.
- Paterson, N. R., and V. Ronka, 1971, Five years of survey with the very low frequency electromagnetic method: Geoexploration, vol. 9, p. 7-26
- Sauck, W.; Sultan, M. Milewski, A., Laton, R., Foster, J., 2009, Integrated Geophysical, Remote Sensing, GIS, and Field Investigations in the Mojave Desert. Project Report: Western Michigan University, Department of Geosciences
- Smith, G., Pimentel, I., 1998, Regional Water Table (1998) and Groundwater-Level Changes in the Mojave River and the Morongo Ground-Water Basins, San Bernardino County, California: USGS Water-Resources Investigation Report 00-4090.

- Stamos, C., Martin, P., Nishikawa, T., and Cox, B., 2001, Simulation of Ground-Water Flow in the Mojave River Basin, California: USGS Water-Resources Investigations Report 01-4002 Version 3
- Stamos, C., Cox, B., Izbicki, J., Mendez, G., 2003, Geologic Setting, Geohydrology and Ground-Water Quality near the Helendale Fault in the Mojave River Basin, San Bernardino County, California: USGS Water-Resources Investigations Report 03-4069.
- Sultan, M., Wagdy, A., Manocha, N., Sauck, W., Gelil, A., Youssef, A.F., Becker, R., El Alfy, Z., Jones, C., 2007, An integrated approach for identifying aquifers in Transcurrent fault systems: The Najd shear system of the Arabian Nubian shield: *Journal of Hydrology*, vol. 349, p.475-488.
- Telford, W. M., Geldart, L. P., and Sheriff, R. E., 1990, *Applied Geophysics*, 2nd ed., Cambridge Univ. Press, p. 770
- Trayler, C. R., and Koczot, K. M., 1995, Regional Water Table (1994) and Water-Level Changes in the Morongo Basin, San Bernardino County, California: USGS Water-Resources Investigations Report 95-4209.
- United States Geological Survey, 2004, Precipitation History of the Mojave Desert Region, 1893-2001: U.S. Department of the Interior, USGS Fact Sheet 117-03.

Vallée, M., Chouteau, M., and Palacky, G.J., 1992, Effect of temporal and spatial variations of the primary signal on VLF total-field surveys: *Geophysics*, Vol. 57, No. 1, 97-105.